Artur BERNAT, Wojciech KACALAK
POLITECHNIKA KOSZALIŃSKA, WYDZIAŁ MECHANICZNY

Metody całkowania numerycznego pola gradientu w inspekcji wizualnej powierzchni narzędzi ściernych z użyciem *Photometric Stereo*

M.Sc. Artur BERNAT

Received his M.Sc. degree at Technical University of Gdańsk in Electronics, Poland, in 1993r. The main scope of interest within his PhD work is the machine vision and image data processing, used in inference process, adapted to estimation of cutting properties of abrasive tools surfaces.

e-mail: abernat@lew.tu.koszalin.pl

Prof. Wojciech KACALAK

Professor of Fine Mechanics Division on Mechanical Faculty of Engineering on TU of Koszalin. From over 15 years he leads research stuffs, as well as, PhD students. Both staffs are working in artificial neural networks applications to control processes in the machining, in machine vision used in inference of surface topography, and in simulation and visualization of grinding processes.

e-mail: wojciech.kacalak@tu.koszalin.pl

Streszczenie

W tym referacie zaprezentowano pewne schematy sprawnego i niezawodnego numerycznego całkowania przestrzennego zawartości dyskretnego pola gradientu. Przegląd poprzedzono wstępnymi rozdziałami dotyczącymi zagadnień *photometric stereo*, w inspekcji wizualnej rzeczywistych powierzchni, z naciskiem kładzionym na możliwe zastosowania podejścia monoskopowego oraz wieloobrazowego w bezstykowej ilościowej estymacji powierzchni o tak zróżnicowanej strukturze geometrycznej, jakimi są powierzchnie narzędzi ściernych.

Słowa kluczowe: inspekcja wizualna, *Photometric Stereo*, całkowanie numeryczne, rekonstrukcja 3D, powierzchnie narzędzi ściernych.

Numerical gradient field integration methods in task of visual inspection of abrasive tools surfaces by means of *Photometric Stereo*

Abstract

In this paper some schemes of efficient and robust numerical spatial integration of the discrete gradient field contents have been presented. The survey follows introductory chapters, related to photometry stereo problems, in visual inspection of real surfaces, with stress put on possible applications of monoscopic and multiimage approach in contactless quantitative estimation of such textured surfaces, like these of abrasive tools.

Keywords: visual inspection, *Photometric Stereo*, numerical integration, 3D reconstruction, abrasive tools surfaces.

1. Introduction

The general aim of works here presented is to give overview of robust and reliable techniques of contactless estimation of cutting properties of abrasive tools surfaces. For this aim, in this paper, base concepts of Photometric Stereo methods (PSM) will be presented, as some representative approach to the given problem.

Firstly, it has been postulated, that such estimations, should be invariably realised either based on given 3D surface (obtained from within 3D profilometry datasets), or based on recovered surface depth information, due to the applied 3D reconstruction algorithm. Hence, the computer vision techniques have been here adopted. Secondly, it's assumed, that very textured surfaces of abrasive tools should be efficiently reconstructed with use of monoscopic and multiimage approach to the problem of surface imaging and mapping of its topography.

Hence PSM methods are considered, while stereoscopic approach has been here excluded from further considerations. This has been done mainly due to still existing obstacles in data interpretation of correspondence and depth information, embedded within images data disparity. Due to presence of specularities, as well as, occurrences of attached (self-shadowing) and cast (self-masking) shadows, it's decided, that at least 3 directional light sources should be applied in fully controlled surface light illumination.

2. Photometric Stereo, implementation problems

The PSM methods are two-staged 3D reconstruction data processing framework, based on 2D intensity images collected. Within such a dataset of images, during each of the data acquisition steps, a single 2D image is being acquired with simultaneously realised activation of one from several directional light sources, in scheme of their activation: singly and subsequently over the surface regarded. With othoregistration assummed as valid, observed spatial variability of output intensity is generally modelled, as result of interaction between directional parameter L of incidence light illumination, and locally depended N normal vector.

Spatially variable reflectance coefficient ρ renders any single-image approach methods, such as Shape-from-Shading (SFS) useless [1, 2]. Thus, there is substantial need for use of multiimage approach, with firstly provided ρ determination:

$$\rho(x,y) = \left\| \left(\left[L^T \right]_{3xn} \cdot \left[L \right]_{nx3} \right)^{-1} \cdot \left[L^T \right]_{3xn} \cdot \left[I \right]_{nx1} \right\|, \; at \; \|N\| = 1 \quad (1)$$

$$\rho(x,y) = \left\| \left[L^+ \right]_{3xn} \cdot \left[I \right]_{nx1} \right\|, \; at \; \|N\| = 1, \quad (2)$$

and secondly realised determination of vector gradient field contents (in form of normals):

$$\frac{\left[N \right]_{3x1}}{\sqrt{1+p^2+q^2}} = \frac{\left(\left[L^T \right]_{3xn} \cdot \left[L \right]_{nx3} \right)^{-1} \cdot \left[L^T \right]_{3xn} \cdot \left[I \right]_{nx1}}{\rho(x,y)}, \; i \in [1..n]; \; i \notin \{spec, selfmsk, selfshdw\} \quad (3)$$

$$\frac{\left[N \right]_{3x1}}{\sqrt{1+p^2+q^2}} = \frac{\left[L^+ \right]_{3xn} \cdot \left[I \right]_{nx1}}{\rho(x,y)}, \; for \; i \in [1..n], \; with \; i \notin \{spec, selfmsk, selfshdw\} \quad (4)$$

In equations (1), (3) the reflectance coefficient ρ and normal orientation N, respectively, for any (x, y) 2D image locations, are determined accordingly to generalised Moore-Penrose's (MR) matrix pseudoinversion, while in equations (2) and (4) Singular Value Decomposition (SVD) is adopted in task of pseudoinversion of matrix of directional parameters. MR inversion has been widely implemented (see examples [4-5]), while SVD based inversion [5] gives better robustness in 3D reconstruction, realised on set of real 2D intensity images. Both generalised pseudoinversions allow for

using of more, than 3 light sources, with direction matrix, which is in such case generally rectangular.

The most challenging in the whole processing framework is to carefully choose robust numerical integration methods, for the obtained vector gradient field contents. There are scanty resources within available literature (see examples: [6, 7]) on this subject. One very often has to cope with contents of gradient fields, acquired in processing of real 2D images set. Hence, gradient field inconsistency and embedded noise should be taken into account.

The main scope of the works here presented will be narrowed, to methods of robust numerical *spatial* integration of the gradient fields, realised in performing 3D reconstruction for surface visually inspected. Hence, variational *global* approaches to the problem, such as [11, 12], will be here omitted, as their implementations do really perform in cases of regularly shaped surfaces, with recurrently repeated patterns.

3. Survey of basic numerical integration methods implemented

Based on review of Computer Vision literature, one comes to conclusion, that methods for numerical integration of gradient fields are trivial, thus to be neglected in scientific account. However, noisy input dataset with important level of inconsistency, renders the reconstruction process almost impossible. Thus, both non-iterative and iterative methods were sought, in hope of obtaining reliable output results. Below, *our* implementations have been accounted.

There are additional phenomena, which positively adds up to the iterative 3D reconstruction process (such as information propagation of surface heights between two subsequent iterations). Perhaps the most reliable are those approaches to the problem, which are derived from finite order Taylor series expansions of unknown height function $z = f(x, y)$ in dependence of given discrete surface slopes p and q, on X and Y directions, respectively.

$$f(x+dx, y+dy) = f(x,y) + \frac{\partial f(x,y)}{\partial x}dx + \frac{\partial f(x,y)}{\partial y}dy + \frac{1}{2}\left(\frac{\partial^2 f(x,y)}{\partial x^2}\partial x^2 + \frac{\partial^2 f(x,y)}{\partial y^2}\partial y^2\right) \tag{5}$$

In above finite Taylor series expansion of $f(x, y)$ function of x, y two variables, with expressions up to 2nd order, it's decided not to include mixed derivatives terms. Within lattice of discrete gradient field contents, the derived surface height can be rendered as the following:

$$\begin{aligned} z_{i,j} &= z_{i-1,j-1} + \varepsilon \cdot p_{i,j} + \varepsilon \cdot q_{i,j} - \frac{\varepsilon^2}{2}(p_{i+1,j} - p_{i,j} + q_{i,j+1} - q_{i,j}) \\ z^n_{i,j} &= z^{n-1}_{i-1,j-1} + \varepsilon \cdot p_{i,j} + \varepsilon \cdot q_{i,j} - \frac{\varepsilon^2}{2}(p_{i+1,j} - p_{i,j} + q_{i,j+1} - q_{i,j}) \end{aligned} \tag{6}$$

In relationship (5, 1st line) finite discrete approximation of p and q 1st order derivatives, on X and Y directions respectively, gives in the result expansion of unknown z height function in dependence of p and q, for any (i, j) point, currently processed. Iterative formula (5, 2nd line) is also derived, with $z(i, j)$ height values determined from one iteration to another (with ε as a span set between 2 successive discrete data lattice points, on both X and Y directions). This is produced for skew orientation of integration paths. Adding up horizontally and vertically oriented integration paths, one obtains a triplet of mutually crossed 3 paths for each of the points, on lattice of discrete gradient field contents (fig. 1):

$$z^n_{i,j} = \frac{1}{3}(z^{n-1}_{i-1,j-1} + z^{n-1}_{i-1,j} + z^{n-1}_{i,j-1}) + \frac{2}{3}\varepsilon \cdot p_{i,j} + \frac{2}{3}\varepsilon \cdot q_{i,j} + \frac{\varepsilon^2}{3}(p_{i+1,j} - p_{i,j} + q_{i,j+1} - q_{i,j}) \tag{7}$$

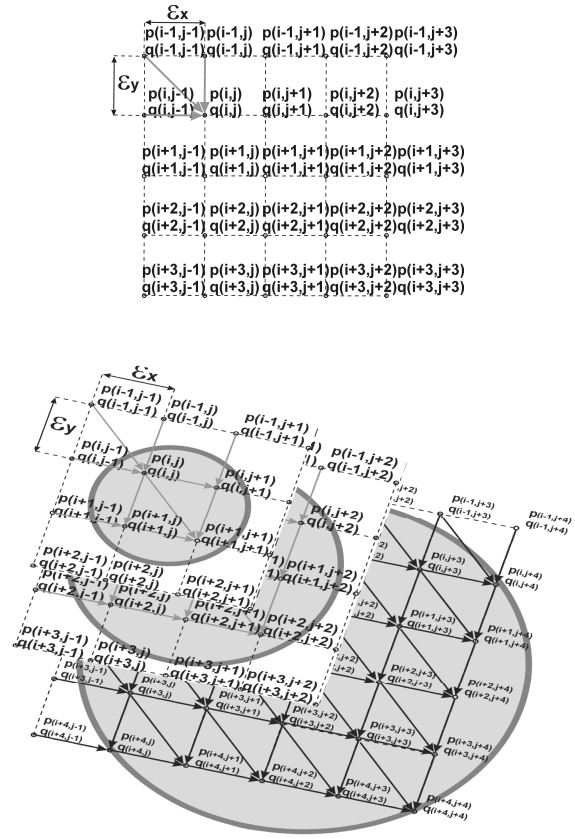

Rys. 1. Po lewej: 3 ścieżki punktowego całkowania, po prawej w kaskadzie: schematy całkowania z maską: 2x2, 3x3, 5x5 elementów branych pod uwagę w ciągu 1 iteracji

Fig. 1. On left: pointwise integration, on right in cascade: mask integration schemes with 2x2, 3x3, 5x5 elements, taken at one iteration

Considering both existing implementations accounted in literature resources [6-10], and the algorithm effectiveness based on *finite* Taylor series expansions accordingly to basic relationship (5) provided with up to 2nd order non-mixed terms, one should underline the accuracy of the later. Coupled, i.e. mixed 2nd order terms could contribute to global and iterative 3D reconstruction process, with the information mainly related to gradient field inconsistency. However, this minor problem should be rather accounted elsewhere.

Coupled 2nd order terms, added to finite series expansion in relationship (5) could represent locally occurred gradient field inconsistency. On other hand, the iterative implementation of the numerical integration method here presented, posses connective character in data interpretation, mainly due to surface height propagation phenomenon. Thus, forcibly any local data inconsistencies are advantageously overwhelmed and suppressed by globally occurred data consistency, related to 2D intensity images dataset for surface visually inspected. Surface height propagation phenomenon plays a role of conveying factor in *omnidirectional* distribution (in XY reference plane for the surface regarded) of height information.

Accordingly to (7) (figure 1 right), there is also possibility to consider more that one location on gradient field, with mask of for example 2x2, 3x3 or 5x5 elements, taken simultaneously at one iteration (here below the case of 2x2 elements mask is presented):

$$\begin{aligned} z^n_{i,j} &= \frac{1}{3}(z^{n-1}_{i-1,j-1} + z^{n-1}_{i-1,j} + z^{n-1}_{i,j-1}) + \frac{2}{3}\varepsilon \cdot p_{i,j} + \frac{2}{3}\varepsilon \cdot q_{i,j} + \frac{\varepsilon^2}{3}(p_{i+1,j} - p_{i,j} + q_{i,j+1} - q_{i,j}) \\ z^n_{i,j+1} &= \frac{1}{3}(z^{n-1}_{i-1,j} + z^{n-1}_{i-1,j+1} + z^{n-1}_{i,j}) + \frac{2}{3}\varepsilon \cdot p_{i,j+1} + \frac{2}{3}\varepsilon \cdot q_{i,j+1} + \frac{\varepsilon^2}{3}(p_{i+1,j+1} - p_{i,j+1} + q_{i,j+2} - q_{i,j+1}) \\ z^n_{i+1,j} &= \frac{1}{3}(z^{n-1}_{i,j-1} + z^{n-1}_{i,j} + z^{n-1}_{i+1,j-1}) + \frac{2}{3}\varepsilon \cdot p_{i+1,j} + \frac{2}{3}\varepsilon \cdot q_{i+1,j} + \frac{\varepsilon^2}{3}(p_{i+2,j} - p_{i+1,j} + q_{i+1,j+1} - q_{i+1,j}) \\ z^n_{i+1,j+1} &= \frac{1}{3}(z^{n-1}_{i,j} + z^{n-1}_{i,j+1} + z^{n-1}_{i+1,j}) + \frac{2}{3}\varepsilon \cdot p_{i+1,j+1} + \frac{2}{3}\varepsilon \cdot q_{i+1,j+1} + \frac{\varepsilon^2}{3}(p_{i+2,j+1} - p_{i+1,j+1} + q_{i+1,j+2} - q_{i+1,j+1}) \end{aligned} \tag{8}$$

In *distant* analogy to Jacobi's iterative solution, one can boost algorithm's convergence, rendering integration process (8) similarly to Gauss-Seidel iterative solution [13]:

$$z^n_{i,j} = \frac{1}{3}(z^n_{i-1,j-1} + z^n_{i-1,j} + z^n_{i,j-1}) + \frac{2}{3}\varepsilon \cdot p_{i,j} + \frac{2}{3}\varepsilon \cdot q_{i,j} + \frac{\varepsilon^2}{3}(p_{i+1,j} - p_{i,j} + q_{i,j+1} - q_{i,j})$$
$$z^n_{i,j+1} = \frac{1}{3}(z^n_{i-1,j} + z^n_{i-1,j+1} + z^n_{i,j}) + \frac{2}{3}\varepsilon \cdot p_{i,j+1} + \frac{2}{3}\varepsilon \cdot q_{i,j+1} + \frac{\varepsilon^2}{3}(p_{i+1,j+1} - p_{i,j+1} + q_{i,j+2} - q^1_{i,j+1})$$
$$z^n_{i+1,j} = \frac{1}{3}(z^n_{i,j-1} + z^n_{i,j} + z^n_{i+1,j-1}) + \frac{2}{3}\varepsilon \cdot p_{i+1,j} + \frac{2}{3}\varepsilon \cdot q_{i+1,j} + \frac{\varepsilon^2}{3}(p_{i+2,j} - p_{i+1,j} + q_{i+1,j+1} - q_{i+1,j})$$
$$z^n_{i+1,j+1} = \frac{1}{3}(z^n_{i,j} + z^n_{i,j+1} + z^n_{i+1,j}) + \frac{2}{3}\varepsilon \cdot p_{i+1,j+1} + \frac{2}{3}\varepsilon \cdot q_{i+1,j+1} + \frac{\varepsilon^2}{3}(p_{i+2,j+1} - p_{i+1,j+1} + q_{i+1,j+2} - q_{i+1,j+1}) \quad (9)$$

As the surface heights propagation is needed, from one iteration step to another, single step of mask integration schemes (8, 9) play an important role in surface heights propagation. In pointwise scheme, this is realised by surface convolution, realised in each iteration step.

4. More evolved schemes of numerical integration methods

In suppressing global falsifications in topography of 3D surface, reconstructed from 2D images of real surface, it's decided to use two alternate sub-iterations in single iterative step.

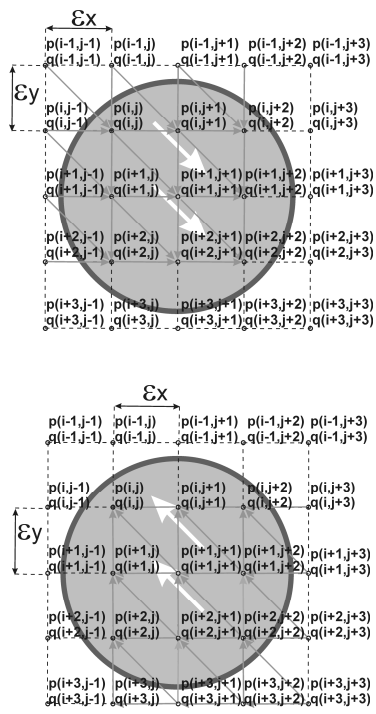

Rys. 2. Po lewej: całkowanie z kierunkiem w dół w 1wszej pod-iteracji, po prawej: całkowanie w górę w 2giej pod-iteracji, pojedynczego kroku iteracyjnego

Fig. 2. On left: integration realised downward in 1st sub-iteration, on right: integration realised upward in 2nd sub-iteration, in single iterative step

Surface deflation, which previously occurred, has been now relaxed, (for macro-topography features on surfaces). In diminishing computational effort, in integration of huge gradient fields, it has been decided to introduce extra algorithm modification. Namely, centres of mask of 3x3 or 5x5 elements are being located more sparsely in global iterations loop, thus reducing considerably global computational effort in 3D reconstruction. In such case, the 3D surfaces resulted are more adequate, indicating better convergence of the reconstruction process. Nonetheless they are characterised by regularly spaced *crust features* on it. These are imperfections of height propagation process, in sparsely implemented schemes of integration.

5. Surface samples inspection and 3D measurements datasets

For test of algorithms performance, distinct surface samples were chosen. First surface was relief of Zloty coin's head (fig. 1), with recognisable pattern on it. Thus, 1st surface sample represents a macro template to be properly mapped, and it is treated, as a test sample in visual inspection/evaluation of the results. Second surface sample was cut from abrasive tape (3M AA237), with aloxite grains impressed into form of pyramids (fig.2). The 2nd sample represents regular occurrence of asperities on surface. Third surface sample is cut from lapping stone, made of red aloxite (fig. 3, description: 99A120MV8).

In case of the 3rd surface sample, one deals with very textured surface. Hence, for random topographic features arrangement on textured surfaces, such as surfaces of abrasive tools, they can be reliably reconstructed with properly adapted *spatial* numerical integration methods, and with the data processing framework in PSM of the solutions posed *spatially*.

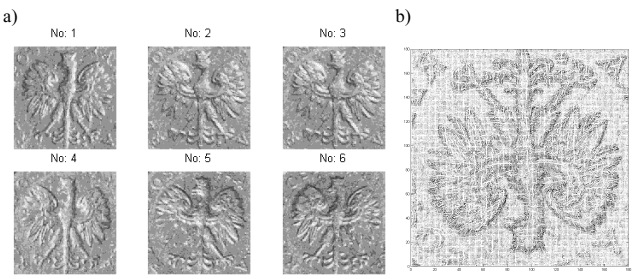

Rys. 3. a) Relief 1 Złotego w oświetleniu o kącie elew. 60 stp., obrazy 2D: 180x180 pikseli, odpow. wym. punktu 83um, b) pole grad. w rekonstr. 3D (współrz. wydruku w środw. Matlab)

Fig. 3. a) Relief: 1 Zloty, light illumination of 60deg of elevation angle, 2D images: 180x180 pixels, pixel spatial correspondence: 83um, b) grad. field in 3Dreconstr.(Matlab coords. plot)

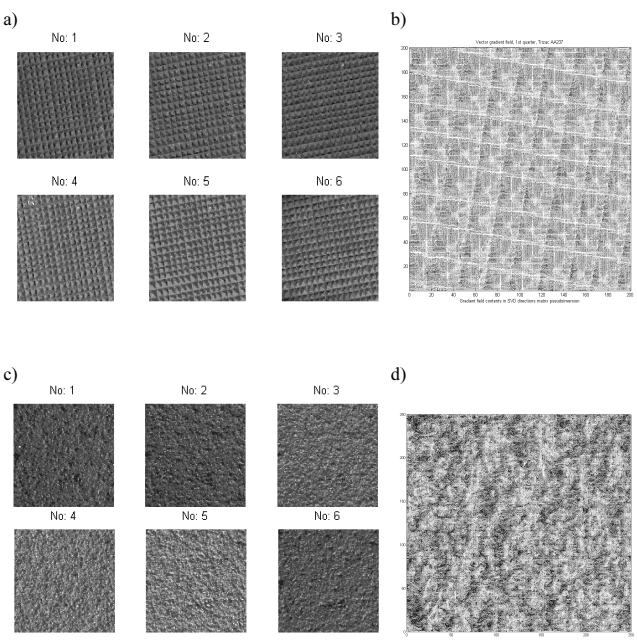

Rys. 4. a) Taśma ścierna (3M AA237), 400x400 pikseli, odp. wym. punktu 10um, b) pole gradientu, c) korund (99A120MV8) kąt elewacji 30 stp., 500x500 pikseli, odp. wym. punktu 14.5um, d) pole gradientu (1wsza ćwiartka) (współrz. w środowisku Matlab)

Fig. 4. a) Abrasive tape (3M AA237), 400x400 pxls, points spatial corresp. 10um, b) gradient field, c) aloxite lapping stone (99A120MV8), incidence light elevation of 30deg, 500x500 pxls, points spatial corresp.: 14.5um, d) gradient field (1st quarter) (Matlab coord. plot)

Though, there exist some global discrete solutions of variationally posed tasks for 3D surface reconstruction, they are narrowed in applications. Such approaches, as in the works of Frankot and Chellapa (*et alli*, see examples of [11, 12]), of globally posed 3D reconstruction problem solved in frequency domain, we have implemented by ourselves and tested. They are proved to be useful in inspection of surfaces of reccurently occurred topography features.

The 2D image datasets for the 3 samples have been acquired with commercially available camera, which is provided with advanced micro-zooming facility, allowing for taking images from minimal object distance of 10 millimetres. As to the 3rd surface samples (fig. 3), it was lit with incidence light of intentionally low elevation angle (30deg.). At such low elevation angle, self-shadowing/self-masking do really occur, but with lowered inter-reflection phenomena. Within set of 2D images dataset, pointwisely realised data classifications and exclusion, render 3D reconstruction scalable, accordingly to number of valid input intensities.

In adapted PSM 3D reconstruction method, in classification and filtering within data pre-processing stage, double-thresholded exclusion has been implemented of arbitrarily set two values. Extremely low output intensities within 2D images are excluded, i.e. treated as invalid data, possibly correlated to self-masking and self-shadowing phenomena. Moreover, extremely high output intensities within 2D images are also excluded, i.e. treated as invalid data, possibly correlated to occurrence of specularities and highlights.

6. Noises and imperfections of real 2D images acquired

Firstly, a valid orientation of triplet of integration paths has been chosen. Gradient field inconsistency of the data occurred due to inherent noise, which induces devastating distortions in 3D reconstruction on one specific skew orientation, while on other direction, the influence of it was diminished considerably. Perhaps, this was provoked by imperfections of acquiring process for intensities data, which can be of non-stationary interline characters within complete scan of the photosensitive cells array.

A *Two Scans* [8, 9] non-iterative integration method is used for testing. It's decided firstly to simulate the presence of noise within synthetic data, at stage of gradient field data processing. The 3D maps from 3D profilometric measurements, for the surface samples were used and treated as a reference *ground truth* data.

Based on simulations realised on synthetic gradient field (2nd surface samples), we noticed, that noise variance of 0.001 or less, embedded within gradient field contents, does not contributes so much to gradient field inconsistency. However, level of the noise variance of 0.02, distinctly alternate results.

It's finally decided to use in comparative analyses, generally the most advanced schemes. That means, the output results of *exclusively* iterative numerical integration methods with both pointwise, and mask schemes with 2x2 and 3x3 elements, were taken into account. Moreover two alternative subiterations (see fig. 2) were applied.

7. 3D surface reconstruction results, comparative analyses

There is an urgent need of some convergence analyses, both in function of number of iterations and computational efforts, spent on particular reconstruction tasks, with overall algorithm performances. However, it's decided, not to realise comparison of absolute max/min height extensions, which in that case should be confronted to *ground truth* dataset.

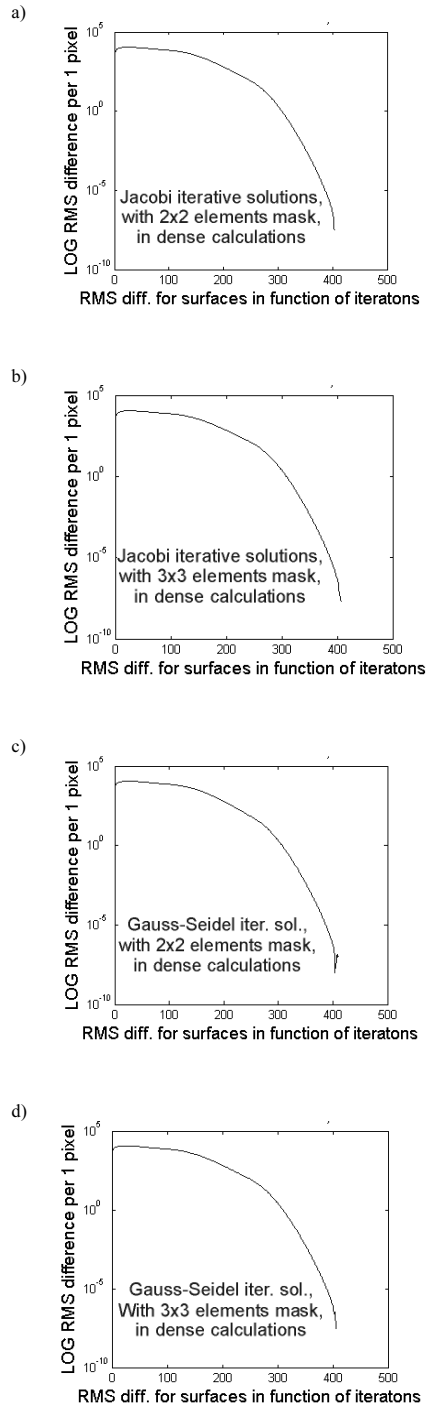

Rys. 5. Różnice RMS kolejnych powierzchni w f. iteracji (próbka 1wsza), schematy maski: a), c) 2x2 oraz: b), d) 3x3 elementy, w rozwiązaniu: a), b) Jacobiego, c), d) Gauss-Seidel'a

Fig. 5. RMS differences for subsequent surfaces in function of iterations (1st sample) mask scheme a), c) 2x2, b), d) 3x3 elements, solutions: a), b) Jacobi, c), d) Gauss-Seidel

Instead of that, the Mean Square Root (RMS) differences between two subsequently reconstructed real surfaces will be presented in function of several aimed numbers of global iterations, spent on them. On figures 5 (a-d) convergence of 3D reconstruction methods is presented, in sense of stabilising the process of the propagation of *z* height information.

The authors tested algorithm implementations, proving stability in presence both of moderate level of the disturbing noise contributing to data inconsistency. For macro-topography templates, it is noticed some intermediate stage of surface heights revolution with final stabilising process after circa 300 iterations.

Finally, the reconstruction results will be presented in brief below for the samples described above in all works here related.

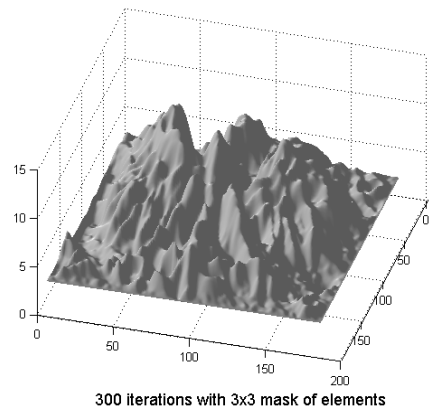

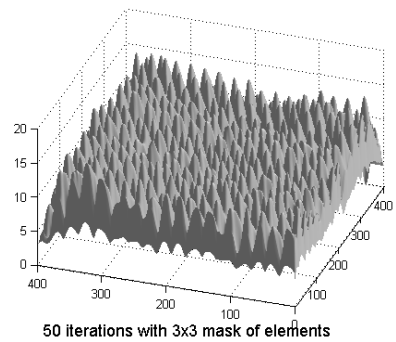

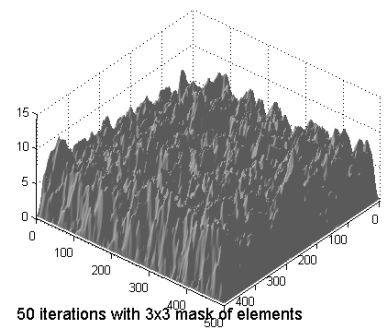

Rys. 6. Wyniki z użyciem rozwiązań iter. Gauss-Seidel dla odpowiednio: 1, 2 i 3 próbki
Fig. 6. Results by Gauss-Seidel iterative solutions for 1st,2nd, 3rd surfaces, respectively

8. A brief critique of possibly existing 3D reconstruction methods and their implications

In pursue of effective 3D surface reconstruction methods, some *unacceptable* solutions and their subsequent implementation implications are accounted in Computer Vision literature. Namely, vector gradient field (see only the example in [6], page 90, subsection 4.3.1: *Filtres moyenneurs* (in French)) is not treated as *oriented*, but mere, as a scalar contents, summed up with use of mean mask, regardless of directions and orientations of the data. In such case one could obtain, quite erratically, only a surface edge detector. Such basic misunderstanding in any numerical integration methods possibly inclines most researches to unnecessary complicated solutions, such as wavelet reconstruction methods, giving up the most basic and probably the most effective methods.

9. Final remarks, conclusions in numerical integration methods

In numerical trials with both real 2D images and depth maps (i.e. taken from 3D prof. measurements), it occurred that surface height propagation played considerable role. Vector gradient field, from its very nature, is of directional contents, and it be should processed exclusively in directional manner, i.e. with use of oriented integration paths (see relationships (6)-(9)). Simultaneously, iterative implementations allow for efficient surface height propagation in all directions on reference plane of the surface visually inspected. Hence, resuming, the iterative implementations prevail over non-iterative ones, in 3D reconstruction.

10. References

[1] Horn B., Brooks M.: The variational approach to shape from shading Computer Vision Graphics and Image Processing, 33(2), pp. 174-208
[2] R.J. Woodham: Photometric methods for determining surface orientation from multiple images. Optical Engineering, 19(1),1980.
[3] M. L. Smith, R. J. Stamp: Automated inspection of texture ceramic tiles. Computers in Industry, (43), 2000, pp.73-82
[4] A. Bernat, W. Kacalak: Problems of determination of stereometry for abrasive tool cutting surface, based on analysis of 2D optical images with use of PS method, V Int. Conf. CMS'05, Cracow, 14-16.XI.2005,Oprogramowanie N-T,Vol.II,p.271-274
[5] A. Bernat A., W. Kacalak: Problems in Derivation of Abrasive Tools Cutting Properties with Use of Computer Vision, Mechatronics 2007, Warsaw,19-21.IX.2007, Recent Advances in Mechatronics, Springer-Verlag, pp.431-437
[6] O. Morel: Environnement Actif Pour la Reconstruction Tridimensionnelle De Surfaces Métalique Spéculaires Par Imagerie Polarimetrique, Thèse Doctorale, Université De Bourgogne 2005
[7] A. Ben Slimane:Caractérisation de texture rugueuses par traitement d'images:application aux revêtements routiers, PhD thesis, Université de Poitiers.
[8] Jr. E. Coleman, R. Jain: Obtaining 3-dimensional shape of textured and specular surfaces using four-source photometry. Comp. Graph. Img. Process.18 (4), pp.309-328
[9] J. Filip: Colour Rough Texture Modelling, PhD thesis, Czech Technical University in Prague, Faculty of Electrical Engineering, Department of Cybernetics, 2005
[10] I. Horovitz, N. Kiryati: Depth from gradient fields and control points: Bias correction in photometric stereo, Img. & Vision Computing, 22(9), pp. 681-694
[11] Frankot R., Chellapa R.: A method for enforcing integrability in shape from shading algorithms, IEEE Trans. Pattern Analysis & Mach.Intell. 10(4), p.439-451, (1988)
[12] T. Wei., R. Kletter:A new algorithm for gradient field integration. Image and Vision Computing New Zealand, Dunedin, pp.22-28
[13] D. Kincaid, Ward Cheney: Numerical Analysis. Mathematics of Scientific Computing, Ed. 3rd, The University of Texas at Austin

Artykuł recenzowany